Micro-Raman scattering in ultrathin-layer superlattices: Evidence of zone-center anisotropy of optical phonons

G. Scamarcio
Dipartimento di Fisica dell'Università di Bari, via Orabona 4, I-70126 Bari, Italy

M. Haines and G. Abstreiter
Walter-Schottky-Institut, Am Coulombwall, W-8046 Garching, Germany

E. Molinari*
Istituto O.M.Corbino, Consiglio Nazionale delle Ricerche I-00189 Roma, Italy

S. Baroni
Scuola Internazionale Superiore di Studi Avanzati, I-34014 Trieste, Italy

A. Fischer and K. Ploog†
Max-Planck-Institut für Festkörperforschung, W-7000 Stuttgart, Germany
(Received 22 July 1992)

Raman spectra of (001) $(GaAs)_m(AlAs)_n$, $1 \leq m, n \leq 7$ superlattices have been measured in backscattering along $\mathbf{x}' \parallel [\bar{1}10]$, $\mathbf{x} \parallel [010]$, and $\mathbf{z} \parallel [001]$ directions with a microprobe. Confined longitudinal (LO) and transverse (TO) optical phonons with $\mathbf{q}$ either parallel or normal to the $\mathbf{z}$ axis have been studied in all the independent scattering geometries. A strong anisotropy is observed when the direction of the transferred momentum is changed from the $\mathbf{z}$ axis to $\mathbf{x}'$ or $\mathbf{x}$. The most evident feature is that the Raman spectra in the $z(x'x')\bar{z}$ geometry are dominated by LO_1 confined phonons, whereas no signal at this energy is present in the $y'(x'x')\bar{y}'$ geometry. Modes evolving from TO_1 and LO_n (n odd) phonons give rise to structures at intermediate frequencies in the $x'(y'y')\bar{x}'$ spectrum. In contrast to LO_1, the measured TO_1 energy remains constant, showing the isotropy of the lower-energy branch of this doubly degenerate mode. These results are explained by microscopic lattice-dynamical calculations performed in an *ab initio* scheme, which properly accounts for angular dispersion and mode mixing. We have also found that in the ultimate limit of confinement, when only one principal mode per branch can be considered, the phonon frequencies can be reproduced by the macroscopic dielectric continuum model, provided that the effect of phonon confinement is considered.

I. INTRODUCTION

Optical phonons in (001) $(GaAs)_m(AlAs)_n$ superlattices (SL's) have been studied in detail both experimentally and theoretically. A good understanding of the main physical properties has been achieved and reviewed in several papers.[1–3] For propagation along the [001] direction, i.e., for wave vector $\mathbf{q}$ forming an angle $\vartheta=0$ with the growth axis, dispersionless confined optical phonons exist. For in-plane propagation ($\vartheta=\frac{\pi}{2}$) the optical phonons acquire significant dispersive character and the so-called macroscopic interface (IF) modes appear. One important theoretical prediction, not yet fully addressed by experiments, is the zone-center anisotropy of infrared active optical modes. At the Γ point of the Brillouin zone, i.e., when $\mathbf{q}\rightarrow 0$ from different directions, their frequency strongly depends on ϑ.[3–9]

Ultrathin layer superlattices (UTLS's), i.e., samples with $m, n \leq 7$ monolayers, have been the subject of special attention because of the ultimate effect of layering on phonons. In UTLS samples strong phonon-confinement effects are observable, which are not only sensitive to the average layer thicknesses but also to interface roughness.[3,10–17] Most experimental investigations on UTLS's have been performed by Raman spectroscopy in the usual backscattering geometry from the (001) surface. In this case momentum conservation and scattering selection rules allow only the observation of longitudinal-optic (LO) phonons propagating along [001]. Although forbidden, IF and transverse-optic (TO) phonons have actually been observed in Raman backscattering from the (001) surface,[18,19] via defect-induced processes, which are particularly effective close to electronic resonances. However, such measurements can only give information about the density of states. They cannot be used to study dispersion or symmetry properties of such modes. Recently, the feasibility of far-infrared reflectivity (FIR) to probe TO-confined phonons propagating along [001] has been demonstrated even in the limit of ultrathin layers.[13,16]

Additional types of measurements are necessary to obtain a full picture of superlattice phonons. In particular, due to experimental limitations, only a limited amount of information is available to date on in-plane propagat-

ing phonons although these modes dominate electron-phonon interaction in confined systems.[20] A suitable method to study in-plane modes of both TO and LO character is micro-Raman spectroscopy, where, taking advantage of the focusing of light to a micrometer-sized spot, backscattering measurements on ($\bar{1}10$) or (010) surfaces can be made. This method has already proven to be successful in studying the in-plane IF phonon dispersion in relatively large period GaAs/AlAs SL's.[21,22]

In this paper, we use micro-Raman spectroscopy to investigate the zone-center optical phonons with wave vector **q** along [010], [$\bar{1}$10], and [001] directions for a number of GaAs/AlAs UTLS's. It is important to stress that in our case, due to the extremely short periods of the samples, the edge of the superlattice Brillouin zone is only a few times smaller than the bulk and therefore the wave vectors of the allowed phonons are effectively at the mini-zone center. We are thus studying the anisotropic nature of the zone-center modes as opposed to dispersion in a particular direction. In addition, the Raman results are compared with previously published FIR measurements on the same samples.[13,16] This allows us to gain an unparalleled amount of information for a set of UTLS samples, where the Γ-point frequencies of both TO and LO modes with **q** parallel or normal to the interface, are measured.

II. EXPERIMENT

The samples have been grown on (001) GaAs substrates by molecular-beam epitaxy. They have been very well characterized by means of x-ray diffraction, Raman scattering, and infrared spectroscopy[13,16] so that it is meaningful to label them with the common notation m/n, m and n being the integer values closest to the actual thickness of the GaAs and AlAs layers. The mean values of the individual layer thicknesses and total superlattice thicknesses are summarized in Table I. Non-integer values of the average number of atomic planes reflect layer thickness fluctuations across the structure. No cap layer was grown, the samples being protected by the last GaAs layer, which was increased to 20 Å for the thinnest cases.

The Raman spectra were measured at a temperature T≈10 K using a triple Dilor XY spectrometer with a focal length of 0.5 m in the additive configuration. The slit widths were set in order to obtain a spectral resolution of 2 cm^{-1}. The 530.9-nm (2.336 eV) line of a Kr^+ laser was used for the excitation. The incident power was kept below 10 mW in order to avoid heating effects. The signal was amplified by a multichannel plate and detected by a Si diode array.

TABLE I. The structure parameters of the $(GaAs)_m(AlAs)_n$ superlattice samples.

Sample	m (ML)	n (ML)	Total SL thickness (μm)
2/1	2.5	1.1	0.25
2/4	2.1	3.7	0.28
3/3	2.8	3.3	2.03
7/7	7.5	6.8	0.50

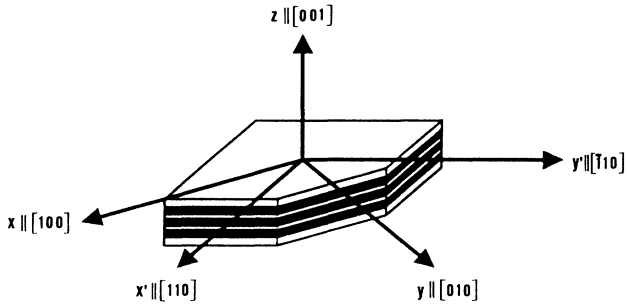

FIG. 1. Schematic diagram of a superlattice grown along [001] showing the convention used in the text for labeling principal axes.

We use the following labels to identify relevant directions with respect to the conventional zinc-blende primitive cell axes (see Fig. 1 for clarity): **z**||[001], **x**||[100], **y**||[010], **x'**||[110], **y'**||[$\bar{1}$10]. The spectra were taken in backscattering geometries from the sample surface (**q**||**z**) and from the sample edge (**q** || **x**, **x'**). In backscattering from the edge a microscope objective is used both for focusing and collecting light; typical spot diameters of about 1 μm or less were achieved. The measured faces were cleaved (**q** || **x'**) or polished (**q**||**x**) parallel to the layer normal. The incident photon polarization was rotated by means of a half-wavelength plate. Because of the low scattering efficiency typically measured off resonance no analyzer was placed in front of the entrance slit of the spectrometer. However, the polarization selectivity of the collection system at 530 nm is measured to be 8:1 and is therefore sufficient to analyze the polarization of the scattered light. The selectivity arises predominantly from the holographic gratings but also from the beam splitter. The scattering configurations are labeled according to the usual Porto notation.[23]

Due to the typical thickness of the SL regions, which are 2 to 3 times smaller than the spot diameter, scattering by the substrate (bulk) cannot be avoided. However, no superposition exists in the AlAs region between the substrate and superlattice modes. In the GaAs region, the bulk LO phonon appear always distinct from the superlattice modes so that the different contributions can easily be separated. The bulk TO mode, which is allowed for (**q** || **x**, **x'**), can obscure GaAs-like superlattice modes. The bulk signals can also be useful to check the energy calibration. In the figures they are labeled with asterisks.

III. INFLUENCE OF ZONE-CENTER ANISOTROPY ON THE RAMAN SPECTRA OF UTLS'S

The gross feature of the anisotropic behavior at the zone center (**q**→0) of the principal optical mode can be qualitatively understood even in a simple dielectric continuum model (DCM).[4,5] However, in the case of UTLS where higher-order confined phonons may play a signifi-

cant role, a true description of the angular dispersion can be achieved to date only in the framework of a microscopic model.[7,6,3] We have performed lattice-dynamical calculations in an *ab initio* scheme based on interatomic force constants obtained within a linear-response density-functional technique,[3,10,24] assuming a perfectly ordered atomic arrangement of the interfaces.

The details of the angular dispersion are quite complicated, but display the following general features, which are easily recognized in the theoretical dispersions shown in Fig. 2. Due to their large total dipole moment, the nodeless $n = 1$ principal modes have the largest angular dispersion for $\vartheta \to 0$. As the **q** direction deviates from **z** towards **x**, the TO_1 modes split into two branches, one dispersionless and the other showing an upward dispersion, and the LO_1 mode energy starts to decrease. When the energy becomes close to that of a mode with the same parity (odd-numbered modes) the two modes mix with each other. As a consequence, LO_n with n odd can acquire significant dispersive character in certain angular ranges; TO_1 and the lowest energy LO_n (n odd) mode may hybridize for **q** lying in the [**x**,**y**] plane. No interaction can occur with even-numbered modes which remain dispersionless. Due to the mixing, a meaningful classification of modes in terms of polarization and quantum numbers is appropriate only for $\mathbf{q}\|\mathbf{z}$. In the following we will adopt the convention of labeling each mode branch by its usual name at ϑ=0. As a result of dispersion with ϑ and breaking of degeneracy of TO_1 modes, the set of $2N$ distinct phonon frequencies $\{TO_n,LO_n\}$ existing for $\mathbf{q}\|[001]$—out of which N are nondegenerate (LO_n) and N are doubly degenerate (TO_n)—is substituted by a different set of $2N+1$ distinct frequencies for $\mathbf{q}\|[\mathbf{x},\mathbf{y}]$. LO_1 is no longer at the highest energy for $\vartheta = \frac{\pi}{2}$, as illustrated in Fig. 2. From the above arguments the following major features in the Raman spectra are to be expected.

(1) For ϑ=0 [$z(--)\bar{z}$ geometries], a strong LO_1 signal with weaker scattering from higher-order LO_n.

(2) For $\vartheta = \frac{\pi}{2}$, [$x(--)\bar{x}$ and $x'(--)\bar{x}'$ geometries], no signal is expected at the $LO_1(\vartheta$=0) energy.

(3) The frequencies of the LO_n modes with n even should be the same for ϑ=0 or $\vartheta = \frac{\pi}{2}$.

The scattering intensities of modes depend on the phonon symmetry and the type of electron-phonon interaction. For ϑ=0 this means the deformation potential for odd-numbered modes and the Fröhlich potential for even-numbered modes.[1,25] Forbidden modes can, however, appear due to disorder. With these considerations in mind we discuss our experimental results.

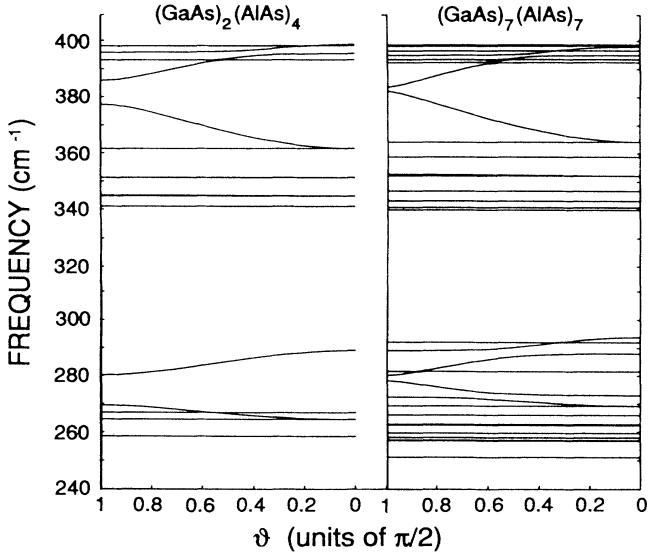

FIG. 2. Calculated angular dependence of zone-center (**q**=0) optical modes for 2/4 and 7/7 samples. ϑ is the angle formed by the phonon wave vector **q** and the growth axis so that $\vartheta = 0$ means $\mathbf{q}\|[001]$ direction whereas $\vartheta = \frac{\pi}{2}$ means in-plane **q**.

IV. RESULTS AND DISCUSSION

The experimental spectra of the investigated UTLS's are displayed in Figs. 3–7. Several important features are common to the whole set of samples and may be best described by referring to the spectra of sample 2/1 (Fig. 3) which possesses the simplest structural and hence vibrational configuration. In this case, due to the ultimate thickness of the AlAs layer (1 ML), only one LO and two TO AlAs-like branches exist. Let us examine first the AlAs region and focus on the phonons having $\mathbf{q} \parallel \mathbf{z}$.

For comparison, Fig. 3(a) shows the far-infrared reflec-

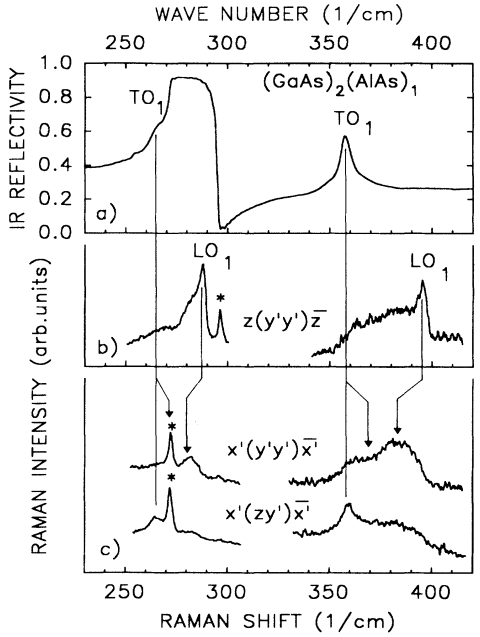

FIG. 3. Comparison between different vibrational spectra measured at $T = 10$ K for the 2/1 sample: (a) far-infrared reflectivity spectrum from Ref. 16; (b) and (c) Raman spectra in backscattering from the (001) surface, and from the cleaved edge, respectively. The scattering configurations are indicated using the labels of Fig. 1. The arrows mark the calculated phonon frequencies according to the dielectric continuum model as explained in the text. The bands labeled by asterisks are due to scattering of bulk GaAs phonons in the substrate.

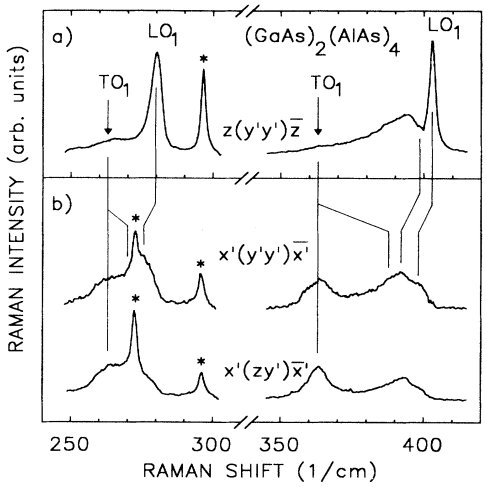

FIG. 4. Raman spectra of sample 2/4 in backscattering from the (001) surface (a), and from the cleaved edge (b). The scattering configurations are indicated using the convention of Fig. 1. The bands labeled by asterisks are due to scattering of bulk GaAs phonons in the substrate. The arrows mark the frequencies of TO_1-confined phonons as measured in Ref. 16. The continuous lines are guides for the eye.

tivity spectrum recorded in near-normal incidence. A detailed description of the "Reststrahlen" bands of UTLS has been reported elsewhere.[13] We just recall that because of the appropriate choice of the total thickness of the investigated SL's, the peak of the AlAs-like "Reststrahlen" band occurs at the frequency of AlAs-like TO_1 confined phonon. Hence, the peak at 357.7 cm^{-1} corresponds to the TO_1 confined phonons with **q** along **z** and in-plane polarization.

The Raman spectrum of sample 2/1 in the $z(y'y')\bar{z}$ configuration [Fig. 3(b)] shows a peak at 395.3 cm^{-1} which is assigned to the AlAs-like LO_1 phonon on the basis of the energy position and scattering selection rules. No additional peak can be observed in the range of AlAs-like phonons. The low-energy tail to the LO_1 band in the $z(y'y')\bar{z}$ Raman spectrum, extending down to about 360

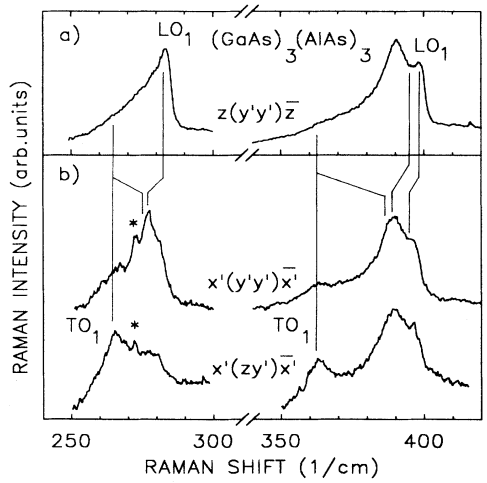

FIG. 5. Same as Fig. 4 for sample 3/3.

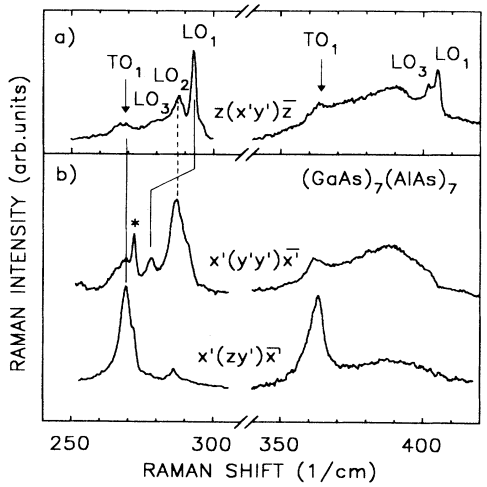

FIG. 6. Same as Fig. 4 for sample 7/7.

cm^{-1}, is a minor feature always observed in UTLS's. It is ascribed to defect-activated optical modes or alloy scattering.

A drastic change in the spectrum is observed when the direction of the transferred momentum is changed from **z** to **x'**. In the topmost trace of Fig. 3(c), recorded in the $x'(y'y')\bar{x}'$ geometry, no signal can be observed at 395.3 cm^{-1}. Instead, a broad band centered at 383 cm^{-1} rises. Hence, the spectra $z(y'y')\bar{z}$ and $x'(y'y')\bar{x}'$ are very different although they share the same polarization configuration and thus the same symmetry-selection rules.

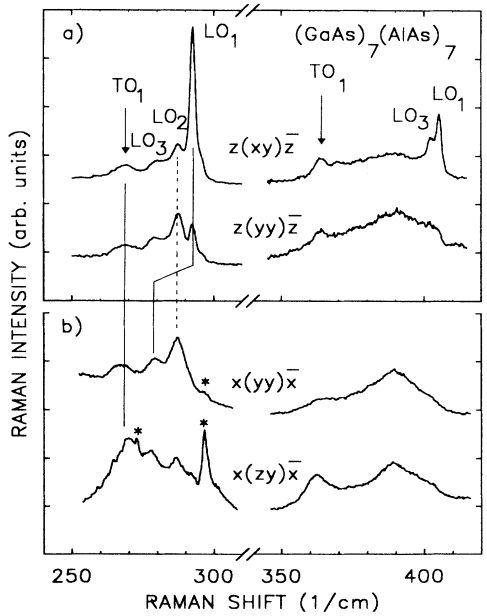

FIG. 7. Raman spectra of sample 7/7 in backscattering from the (001) surface (a), and from the polished edge (b). The scattering configurations are indicated using the convention of Fig. 1. The bands labeled by asterisks are due to scattering of bulk GaAs phonons in the substrate. The arrows mark the frequencies of TO_1 confined phonons as measured in Ref. 16. The lines are guides for the eye.

The differences between them arise predominantly as a result of the different wave vector directions. This behavior is clear evidence of the anisotropy of zone-center LO phonons.

For the depolarized micro-Raman spectrum $x'(zy')\bar{x}'$, the spectral line shape changes further. The spectrum is dominated by a peak at 359.1 cm^{-1}. According to the energy position and scattering selection rules, this peak can be ascribed to TO_1 confined phonons propagating in plane.

Now turning to the GaAs region, a similar behavior can be observed. The peak at 288 cm^{-1} in the $z(y'y')\bar{z}$ spectrum is due to the GaAs-like LO_1 confined phonon with $\mathbf{q} \parallel \mathbf{z}$. This peak disappears in the $x'(y'y')\bar{x}'$ spectrum where it is replaced by the band at 281.6 cm^{-1}. The peak at 264.6 cm^{-1} in the $x'(zy')\bar{x}'$ spectrum and the shoulder at 263 cm^{-1} in the FIR spectrum are due to the TO_1 phonons propagating along the $\mathbf{x}'$ and $\mathbf{z}$ directions, respectively. The frequencies of higher-order LO_2 and TO_2 phonons are expected to fall at frequencies lower than TO_1 in this sample. However, no important structure can be observed in this range because of the reduction in the scattering efficiency with increasing order, and due to the off-resonance condition.

By comparing the different spectra in Fig. 3, it is seen that the TO and LO superlattice phonons have dissimilar angular dependencies. In contrast to the anisotropic behavior of LO modes, no energy difference exists between TO_1 confined phonons with the wave vector parallel and perpendicular to the $[x, y]$ plane. The strong signal measured either in Raman or in FIR spectra is evidence that this mode retains its even-parity nodeless nature.

The broad bands at 383 and 365 cm^{-1} in the $x'(y'y')\bar{x}'$ spectrum are likely to be due to the superposition of two contributions related to modes which evolve from the LO_1 and TO_1 confined phonons with $\mathbf{q} \parallel \mathbf{z}$. These two modes appear unresolved even if a rather large separation is expected (about 8 cm^{-1}), which is much larger than the spectral resolution or the temperature broadening. We ascribe the observed broadening to the existence of structural disorder which breaks the translational symmetry and allows scattering by phonons with $\mathbf{q}$ in a broad range of values around the allowed $\mathbf{q} = \mathbf{k}_{in} - \mathbf{k}_{out} \approx \mathbf{0}$. Disorder-induced scattering of phonons with $\mathbf{q} \neq \mathbf{0}$ becomes weakly allowed. Hence the observed line shape is somehow related to the phonon density of states.

The main effects of the anisotropy of the zone-center optical phonons in SL's are also clearly observed in the Raman spectra of Figs. 4–6 for samples 2/4, 3/3, and 7/7. The assignments of the various spectral features are obtained on the basis of phonon-energy calculations and polarization properties as indicated on the figure. In particular, the strong and sharp LO_1 peaks observed in the $z(y'y')\bar{z}$ geometry disappear in the $x'(y'y')\bar{x}'$ spectra. Another feature which is seen throughout is that the lowest-energy TO_1 mode can be observed both in the $x'(zy')\bar{x}'$ Raman and in the FIR spectra at the same energy, thus confirming that this branch is isotropic. The change in the layer thicknesses causes several changes in the spectral features: the peak positions of the $n = 1$ principal modes shift in the different spectra as a function of the phonon well width and higher-order modes appear in the spectra. Modes evolving from TO_1 and LO_n (n odd) phonons give origin to structures at intermediate frequencies in the $x'(y'y')\bar{x}'$ spectrum.

For the 7/7 sample there are additional results from the polished (010) edge along with comparable measurements from the (001) surface as shown in Fig. 7. Concentrating on the GaAs region it is seen that LO_1 (292.9 cm^{-1}) and LO_2 (286.8 cm^{-1}) modes dominate the $z(xy)\bar{z}$ and $z(yy)\bar{z}$ spectra, respectively, in accordance with well-known scattering selection rules in superlattices. The observation of residual signals due to LO_1 and LO_2 modes in their respective forbidden polarization can be partly ascribed to the imperfect polarization selectivity of gratings or to the proximity of resonance with high index optical transitions.

Once again no signal is observed at the $LO_1(\vartheta{=}0)$ frequency for in-plane scattering. The strongest peak in the $x(yy)\bar{x}$ spectrum, which coincides in energy with the $LO_2(\vartheta{=}0)$ mode, corresponds to $LO_2(\vartheta = \frac{\pi}{2})$. This is related to the dispersionless character of the even-numbered LO_n modes and their anticrossing with dispersive LO_1 phonon. The bands at 278 and 270 cm^{-1} are particularly evident in the $x(zy)\bar{x}$ spectrum. The former can be ascribed to modes evolving from LO_1, the latter to modes evolving from LO_3, TO_1, and LO_5 phonons according to the calculated angular dispersion. In the AlAs region the two peaks in the $z(xy)\bar{z}$ spectrum are substituted by a broad band peaked at 388 cm^{-1}. Several contributions, here unresolved, come from the large number of modes falling in the considered wave-number range. However, considering the theoretical predictions for this particular sample, the peak at 388 cm^{-1} can be ascribed to modes evolving from TO_1 and the lowest-energy LO_7 phonons.

We now come to a more detailed comparison with theory. As highlighted in Sec. III, only a fully microscopic model of superlattice dynamics can account for the combined effects of confinement and mode mixing in UTLS's, though a quantitative comparison between experiment and theory will need consideration of cationic intermixing processes at the GaAs/AlAs interfaces.[10] Bare macroscopic models fail to reproduce the experimental results from the qualitative as well as from the quantitative point of view because phonon dispersion and hybridization of modes cannot be accounted for.[26] However, we have found that in the ultimate limit of confinement, i.e., when only one principal mode per branch needs to be considered, it is possible to reproduce the measured phonon frequencies with great accuracy in the framework of a macroscopic approach, if we properly take into account the effect of confinement as outlined in Ref. 27. For instance, in the case of the 2/1 sample, neglecting the contribution from $n = 2$ GaAs-like optical modes, the dielectric function of GaAs or AlAs slabs can be written in the following classical form:[27]

$$\epsilon = \epsilon_\infty \frac{\omega^2 - LO_1^2}{\omega^2 - TO_1^2}, \tag{1}$$

but substituting the bulk-phonon frequencies with the

experimental frequencies TO_1 and LO_1 of confined optical phonons measured for $\vartheta=0$. In the framework of the dielectric continuum model, the angular dispersion of $\mathbf{q}\rightarrow 0$ phonons is expressed by

$$\left(\frac{\epsilon_G(\omega)+\epsilon_A(\omega)}{\epsilon_G(\omega)-\epsilon_A(\omega)}\right)^2=\cos(\vartheta)^2+\left(\frac{d_A-d_B}{d_A+d_B}\right)^2\sin(\vartheta)^2. \tag{2}$$

The position of the arrows in Fig. 3 have been calculated according to the above equations. The excellent agreement between theory and experiment shows the power of combining macroscopic with microscopic considerations when no mixing of modes takes place. This has already been succesful to analyze FIR measurements from UTLS.[16]

V. CONCLUSION

Our experimental data provide direct evidence of zone-center anisotropy of optical phonons in GaAs/AlAs superlattices. In particular, when the direction of the phonon wave vector $\mathbf{q}$ is changed from the $\mathbf{z}$ axis to the $[x,y]$ plane, the frequency of LO_1 principal modes is strongly redshifted, whereas the TO_1 modes, which are degenerate at $\vartheta=0$, split into two branches, one is blueshifted and the other remains constant in energy. Modes evolving from TO_1 and LO_n (n odd) phonons give rise to structures at intermediate frequencies. This behavior is explained by microscopic *ab initio* lattice-dynamical calculations which properly consider the angular dispersion and mixing with higher-order modes with the same parity. One important finding is that, in the ultimate limit of confinement, when only one principal mode per branch can be considered, the phonon frequencies can be reproduced by the macroscopic dielectric continuum model, provided that the effect of phonon confinement is considered. We believe that the present investigation of Γ-point optical phonons with in-plane wave vector is important not only to complete the picture of phonons in UTLS, but also because these modes play a crucial role in the electron-phonon interaction in confined systems.

ACKNOWLEDGMENTS

Part of this work was supported financially by Deutsche Forschungemeinschaft (Grant No. SFB 348). This work was partially supported by Italian CNR and MURST. Calculations were supported by CNR under Grants No. 91.00658.PF69 and No. 91.00653.PF69.

*Present and permanent address: Dipartimento di Fisica, Università di Modena, via Campi 213/A, I-41100 Modena, Italy. Electronic address: molinari@imovx2.unimo.it

†Present address: Paul-Drude-Institut für Festkörperelektronik, O-1086 Berlin, Germany.

[1] B. Jusserand and M. Cardona, in *Light Scattering in Solids V*, edited by M. Cardona and G. Güntherodt, Topics in Applied Physics Vol. 66 (Springer, Berlin, 1989).

[2] J. Menéndez, J. Lumin. **44**, 285 (1989).

[3] E. Molinari, S. Baroni, P. Giannozzi, and S. de Gironcoli, in *Proceedings of the 20th International Conference on the Physics of Semiconductors, Thessaloniki, 1990*, edited by E. Anastassakis and J. Joannopoulos (World Scientific, Singapore, 1990), p. 1427.

[4] M. Cardona, in *Spectroscopy of Semiconductor Microstructures*, edited by G. Fasol, A. Fasolino, and P. Lugli (Plenum, New York, 1991).

[5] M. Cardona, Superlatt. Microstruct. **5**, 27 (1989).

[6] S. Ren, H. Chu, and Y. Chang, Phys. Rev. Lett. **59**, 1841 (1987); Phys. Rev. B **37**, 8899 (1988).

[7] E. Richter and D. Strauch, Solid State Commun. **64**, 867 (1987).

[8] L. Miglio and L. Colombo, Surf. Sci. **221**, 486 (1989).

[9] H. Gerecke and F. Bechstedt, Superlatt. Microstruct. **9**, 173 (1991).

[10] E. Molinari, S. Baroni, P. Giannozzi, and S. de Gironcoli, Phys. Rev. B **45**, 4280 (1992).

[11] D. Kechrakos, P.B. Briddon, and J.C. Inkson, Phys. Rev. B **44**, 9114 (1991).

[12] B. Jusserand, Phys. Rev. B **42**, 7256 (1990).

[13] G. Scamarcio, E. Molinari, L. Tapfer, M. Lugarà, and K. Ploog, Surf. Sci. **267**, 430 (1992).

[14] B. Jusserand, F. Mollot, R. Planel, E. Molinari, and S. Baroni, Surf. Sci. **267**, 171 (1992).

[15] J. Grant, J. Menéndez, L.N. Pfeiffer, K.W. West, E. Molinari, and S. Baroni, Appl. Phys. Lett. **59**, 2859 (1991).

[16] G. Scamarcio, L. Tapfer, W. König, A. Fischer, K. Ploog, E. Molinari, S. Baroni, P. Giannozzi, and S. de Gironcoli, Phys. Rev. B **43**, 14 754 (1991).

[17] D. Gammon, B.V. Shanabrook, and D.S. Katzer, Phys. Rev. Lett. **67**, 1547 (1991).

[18] R. Merlin, C. Colvard, M.V. Klein, H. Morkoc, A.Y. Cho, and A.C. Gossard, Appl. Phys. Lett. **36**, 43 (1980).

[19] A.K. Sood, J. Menéndez, M. Cardona, and K. Ploog, Phys. Rev. Lett. **54**, 2115 (1985).

[20] H. Rücker, E. Molinari, and P. Lugli, Phys. Rev. B **45**, 6747 (1992).

[21] R. Hessmer, A. Huber, T. Egeler, M. Haines, G. Tränkle, G. Weimann, and G. Abstreiter, Phys. Rev. B **46**, 4071 (1992).

[22] A. Huber, T. Egeler, W. Ettmüller, H. Rothfritz, G. Tränkle, G. Weimann, and G. Abstreiter, Superlatt. Microstruct. **9**, 309 (1991).

[23] See, e.g., W. Hayes and R. Loudon, *Scattering of Light by Crystals* (Wiley, New York, 1978).

[24] S. Baroni, P. Giannozzi, and E. Molinari, Phys. Rev. B **41**, 3870 (1990).

[25] K. Huang, B. Zhu, and H. Tang, Phys. Rev. B **41**, 5825 (1990).

[26] B. Zhu, Phys. Rev. B **38**, 7694 (1988).

[27] H. Chu and Y.C. Chang, Phys. Rev. B **38**, 12 369 (1988).